Atomic and Electronic Structure of a Dissociated 60° Misfit Dislocation in $Ge_xSi_{(1-x)}$

P. E. Batson

IBM Thomas J. Watson Research Center, Yorktown Heights, New York 10598

(Received 23 July 1999)

Electron energy loss spectroscpy (EELS) spectra and atomic column images were obtained from a dissociated 60° misfit dislocation at the Ge_xSi_{1-x} substrate interface of a strained Si quantum well. Silicon $2p_{3/2}$ EELS spectra from the stacking fault show splitting of the L_1 conduction band minimum caused by third-neighbor interactions at the fault. Spectra from the 30° dislocation show a similar splitting as well as in-gap defect electronic states. Spectra from the 90° dislocation also show evidence of in-gap states but do not show the L_1 splitting. An extended core structure based on a double period pairing reconstruction may be able to explain this lack of L_1 splitting.

PACS numbers: 78.40.Fy, 61.72.Bb, 61.72.Ff, 61.72.Lk

It has been accepted for many years that dislocation/stacking fault defects in silicon support electrically active states within 0.1 eV of the conduction band (CB) minimum [1,2]. Transmission electron microscopy and luminescence studies of deliberately deformed silicon have confirmed optical activity near the defect, but the atomic structure that gives rise to the activity is not yet known [3–7].

Misfit dislocations at heterojunctions also dissociate into similar dislocation/stacking fault structures, and have been suspected to contribute to limited electron mobility in strained $Si/Ge_xSi_{(1-x)}$ heterostructures [8]. Optical activity has also been detected associated with these structures [9].

Although core structures are not known, most theoretical work with likely structures has found little reason for optical activity at either the stacking fault [10–12], or at straight partial dislocations bounding the fault [13–15]. In fact, straight 30° dislocation cores appear likely to reconstruct, largely clearing the conduction band gap of deep states [14]. Recent studies of 90° core structures also find that they are likely to reconstruct to lower their total energy [16,17]. Finally, there has been some theoretical evidence for shallow valence band states [18].

I report spatially resolved electron energy loss spectroscopy (EELS) measurements from dissociated misfit dislocations in a strained Si quantum well imbedded in $Ge_{0.35}Si_{0.65}$. These results show the local CB at the 30° dislocation ($P30$), the intrinsic stacking fault (ISF), and the 90° dislocation ($P90$). The structure and the spatial location for the spectra are obtained using annular dark field (ADF) imaging with a 0.2 nm resolution in the VG Microscopes, scanning transmission electron microscope (STEM) [19,20]. The Wien Filter EELS spectrometer had a 160 meV energy resolution with a ± 20 meV reproducibility [21,22]. Since the field emission source has an energy spread of 0.3 eV, the spectral resolution after numerical deconvolution was limited to about 0.25 eV by statistical considerations [23].

The dissociated 60° misfit dislocation structures occurred at the substrate interface of a 15 nm thick Si quantum well structure, deliberately engineered to investigate the effect of misfit dislocations on carrier mobility [8]. It is believed that the the dislocation location and structure are established during growth at 500 °C–550 °C, and can be regarded as stationary during specimen preparation at room temperature. Figure 1 shows an ADF image after applying a 0.15 nm smoothing filter to reduce measurement noise. The image is a [1 −1 0] projection of the [0 0 1] substrate/well interface (dashed line). In this image, Si-Ge atom columns are arranged in pairs separated by 0.14 nm in the [0 0 1] direction, appearing as elongated spots using the 0.2 nm diameter STEM probe.

The 60° dislocation dissociates into a $P30$ dislocation located within the substrate/well interface, a stacking fault lying in a (1 1 1) plane extending into the substrate, and a $P90$ dislocation within the alloy substrate. The measured distance between the two partial dislocations is 3.3 nm, or 10 "dumbbell" units. The $P90$ structure is not very distinct, due probably to some kinks occurring along its

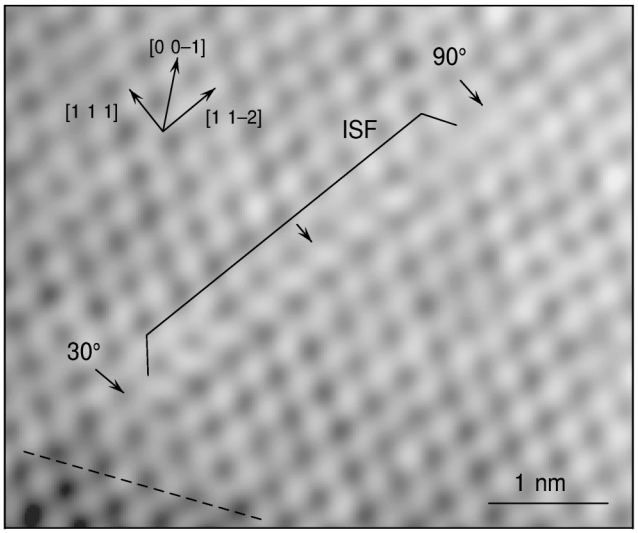

FIG. 1. ADF image of the [1 −1 0] projection of a dissociated 30°/ISF/90° structure at the substrate interface of a strained Si quantum well. The Si interface is indicated by the dashed line.

length [4,24]. However, it can be located by considering the continuity of [1 1 −1]-type atomic planes as they cross the ISF. Inspection of the $P30$ core reveals a very close agreement with the glide-cut structure [13]. The $P90$ core image, however, does not readily agree with the simple (5−7)-fold ring structure, which is not surprising, given our expectation that kinks may be present.

The spatially resolved EELS measurements follow extensive work with relaxed Ge-Si alloys [25,26] and strained quantum wells [27,28]. Raw Si $2p$ core absorption spectra are processed to remove a slowly varying background, to sharpen the energy resolution by deconvolution of the incident beam energy distribution, and to remove the $2p_{1/2}$ core to conduction band intensity. The remaining intensity, due to excitation from the $2p_{3/2}$ core level to the s- and d-projected conduction band local density of states (LDOS), is then fitted with a model spectrum, generated from a trial LDOS, using an inelastic scattering theory including core excitonic interactions, lifetime broadening, and instrumental resolution. The model LDOS consists of parabolic effective mass contributions for the s-like band edges at Δ_1, L_1, and a saddle point at the d-like point L_3. These contributions are terminated linearly at the p-like points $\Gamma_{1,5}$ and $\Gamma_{2'}$ in the center of the Brillouin zone (BZ). The model positions for the important band edges Δ_1 and L_1 are then varied to fit the measured spectrum. When applied to the relaxed Ge-Si alloys, this method allows the composition to be determined within 5% throughout the possible alloy compositions. It also obtains conduction band offsets with an accuracy of ± 20 meV [29]. The analysis does not consider effects due to point defects or impurities which may be present near the defect, but it can be said that all spectral variations observed near the defect could be understood by including effects due to expected local strain.

In Fig. 2, I show Si $2p_{3/2}$ results for the relaxed alloy compared with results from the ISF, $P30$, and $P90$ structures taken from the positions indicated by the arrows in Fig. 1. Each analysis includes the processed data, a modeled LDOS, and the resulting spectral fit. The most striking feature of these spectra is the behavior of the L_1 peak near 101 eV, which splits into two contributions at the ISF. This can be understood using the calculations for Si of Mattheiss and Patel [11]. They predict that the L_1 branch is projected into the center of the 2D hexagonal ISF Brillouin zone, and is then split into two components by the mixing of Si sp^3 orbitals from third-neighbor atoms on either side of the glide-cut plane. A similar mechanism apparently occurs in the II-VI compounds, where the single Γ_1 band minimum in the zinc-blende structure is replaced by two components, Γ_1 and Γ_3, in the wurtzite structure [30]. I model this behavior by introducing a gap in the L_1 band, labeling the upper and lower branches, Γ^+ and Γ^-. This splitting is calculated to be about 1.5 eV for Si, while the lower band is calculated to shift about 0.25 eV down from the L_1 minimum in the bulk. These predictions strongly resemble the observed behavior. The work

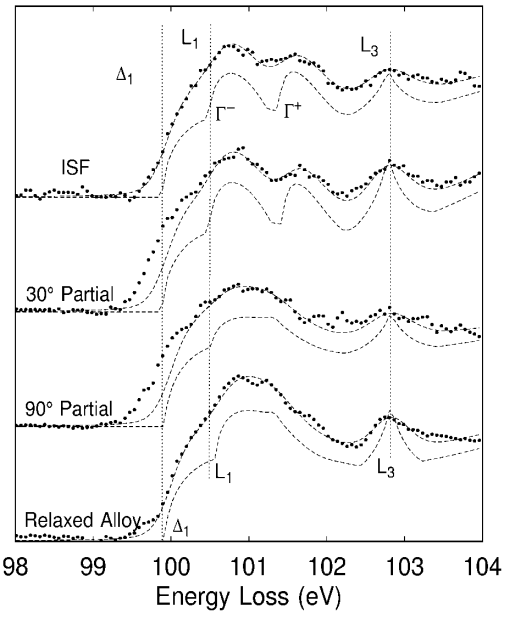

FIG. 2. Si $2p_{3/2}$ spectra from four locations in the dissociated dislocation structure. The L_1 band is split at the ISF into two components. This splitting is present also at the $P30$ core but not at $P90$. Both dislocation cores support near-edge gap states at Δ_1, but the ISF does not.

also predicts that the X_1 CB in the bulk lattice, for which Δ_1 is the band minimum, becomes the Γ-M band in the hexagonal ISF BZ and is not affected by the change in local symmetry at the ISF. Again this is reflected in the data, which shows no change at the ISF Δ_1 onset relative to the bulk alloy.

Results from the $P30$ and $P90$ cores reveal a remarkable result: the L_1 peak is split at the $P30$ core, but not at $P90$. Extra scattering intensity occurs below Δ_1 in each case. This behavior is strong evidence for similarities of atomic structure between the $P30$ and the ISF, on the one hand, and the $P90$ and the bulk, on the other. I have considered likely model dislocation core structures to investigate this, using a local radial distribution function to track the third-neighbor distances and an angular structure factor to characterize the local atomic symmetry. In the Mattheis and Patel calculation, the L_1 splitting is attributed to the shift of one of the third neighbors into a second-neighbor distance. This transforms the bulk Si "chair" structure into a "boat" structure, breaking the local atomic D_{6h}^4 symmetry to produce D_{3d}^3 symmetry. This symmetry breaking can be detected in a model structure by projecting an atom and its third neighbors onto each of the possible four (1 1 1)-type planes and then characterizing the azimuthal position, ϕ, of the atoms with an azimuthal structure factor (ASF) $e^{i3\phi}$. Summation of these factors for the third neighbors yields 0 for a 6-fold, bulklike structure and 6 for a 3-fold ISF-like structure.

The model consists of four (1 −1 0) single atom layers—810 atoms in all—including the whole $P30$-ISF-$P90$ structure. This allows effects due to dislocation induced strain to be included for the ISF. For

the dislocation cores, I have used calculated structures from several sources ($P30$ [14], $P90$ [15,16]). After insertion into the extended model, these structures were adjusted by hand to reproduce the Si-Ge bond length to within $\pm 8\%$. Finally, they were relaxed using a Keating potential with fixed boundaries in the $(1\ -1\ 0)$ plane, chosen to match the imaging data and periodic boundary conditions perpendicular to this plane.

Figure 3 summarizes the results for several local atomic environments within the model. In this figure, I plot third-neighbor distances against the azimuthal structure factor, ASF. In areas having a bulklike environment, the third-neighbor distance is about 0.45 nm with an ASF of 0. The ISF results clearly show some third neighbors in bulk positions (6-fold, ASF $= 0$) and some in the ISF positions at 0.38–0.4 nm with an ASF $= 6$. This third-neighbor behavior was identified by Mattheiss and Patel as the one responsible for the splitting of the L_1 band [11]. The structural characterization technique therefore captures the essential features that affect the electronic behavior—the atomic distances and local symmetry. Continuing with $P30$, using the reconstructed core from Chelikowsky [14], I find that it also has third-neighbor distances and local symmetry characteristic of the ISF, consistent with the finding of a splitting in the L_1 band. A surprise here is that the responsible third neighbors are not located in $[1\ 1\ 1]$ planes as in the ISF, but in $[\ 1\ -1\ 0]$ planes, perpendicular to the core locus, and are a consequence of the pairing reconstruction that clears the gap of deep states. In contrast to the ISF cases, however, several neighbors are in positions which are not characteristic of either the bulk or the ISF. I suggest that these may be responsible for the near-edge in-gap intensity that extends below the CB onset at Δ_1. This would be consistent with the positive deformation potential at the conduction band edge [31].

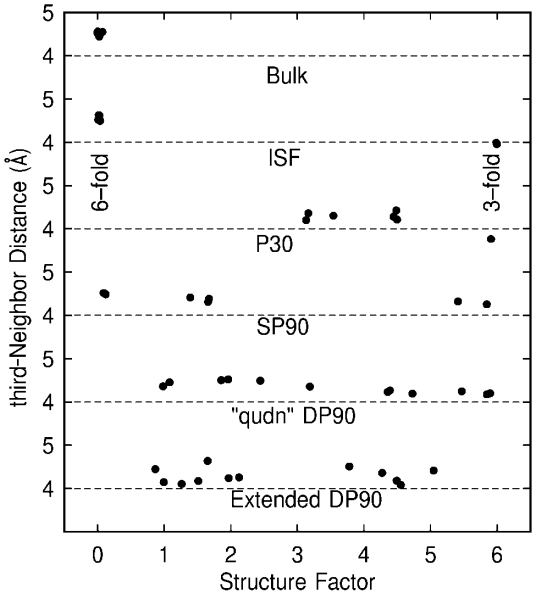

FIG. 3. Third neighbor distances and structure factors for typical atoms located within various types of model structures including the bulk, ISF, reconstructed $P30$ under strain, SP $P90$, qudn DP $P90$, and extended DP $P90$. L_1 splitting is expected when the third-neighbor structure factor and distance match ISF values.

Moving to $P90$, the 5–7 atom ring, single-period (SP) reconstruction has several neighbors in the ISF-like positions. Therefore, the spectral results cannot be explained using this model. A recent proposal by Bennetto *et al.* [16] introduces kinks at every other atom position along the core. I show the "qudn" double period (DP) structure [16], and find that ISF-like positions remain. Finally, in this structure I have used the well-known fact that kinks are pervasive in order to produce an extended core that includes four sets of DP kink structures. This structure eliminates ISF-like atom environments to give agreement with the spectroscopic evidence. In addition, it provides a set of second-neighbor sites which are similar in behavior to those at $P30$, possibly explaining the similarity of the near-edge intensity below the CB edge observed in both cases. It should be remarked that, while these models are periodic along the core, there exist so many kink-related defect structures that the core could appear to be nearly amorphous while preserving the local environment, much as amorphous Si retains a local environment that is similar to crystalline Si.

Returning to the imaging results, I show [in Fig. 4(a)] 0.2 nm resolution imaging data at the $P90$ core, compared with (b) SP, (c) qudn DP, and (d) extended DP models. In the experimental data, I include segments of three intensity contours at 50%, 75%, and 90% to highlight the shape of each double column intensity peak. In the models, I include atom positions and bond connectivity.

Referring to the numbering in Fig. 4(a), columns 4, 6–7, and 9–12 show elongation in the bulklike (0 0 1) direction. Column 5 is elongated in the ISF direction. Columns 1, 2, and 8 appear symmetric. Finally, columns 3 and 7 are ambiguous, neither clearly symmetric nor clearly elongated. Intensity saddle points between 5–6 and 5–9 clearly show the expected ISF structure. At the $P90$ core, the intensity saddle points lie at the midplanes of columns 1, 2, and 7, while column 3 has a saddle point in the symmetric position towards column 10 but in an asymmetric position towards column 4. Inspection of the three model structures shows that the symmetric shape of column 1 at the core is not consistent with the straight SP structure, but does match the two DP models. Of course this is not a strong statement, because a single kink in the SP structure would produce the symmetric image in this projection. On balance, however, the imaging data appears most consistent with an extended structure for the core. The structure considered here gives an image that resembles the experimental image, but probably does not represent a unique choice.

It is interesting to note that the additional kinks may be introduced without transport of material. A simple rotation of atomic pairs suffices and this can be done with manageable bond distortion. In contrast, these structures

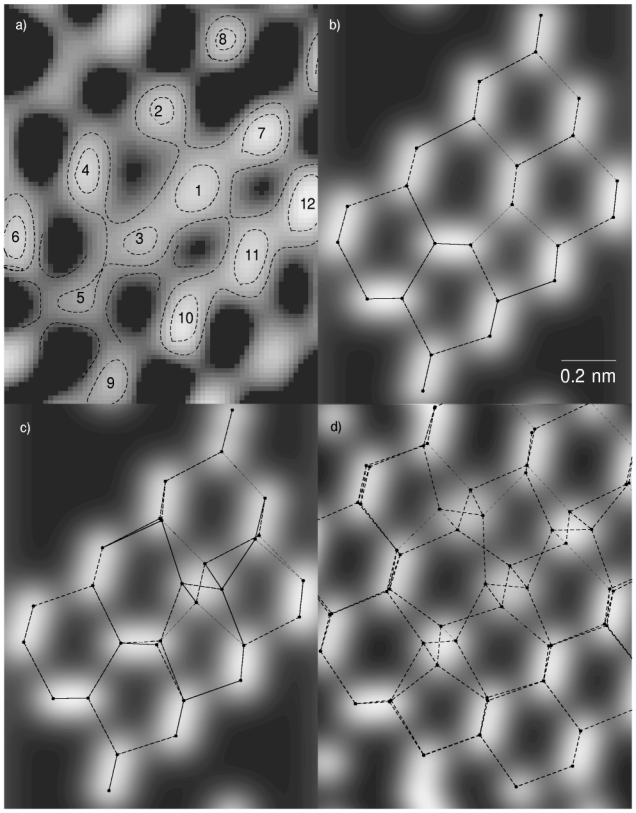

FIG. 4. (a) Experimental $P90$ structure from Fig. 1. Some of the atom column spots are not obviously elongated. (b) SP $P90$ model structure using a 0.2 nm resolution. All spots are elongated in either bulklike or ISF-like directions. (c) DP qudn model structure. The core is not elongated because it consists of equal numbers of bulk and ISF environments. (d) Extended DP structure. Four sets of kinked structures correspond favorably with four symmetric spots in the experimental image.

cannot be introduced at the $P30$ core, because the rotation will bring one atom out of registry with the parent structure due to the presence of the screw component of the 30° partial dislocation. The generation of kinks by pair rotation may therefore contribute to the difference in mobility between $P30$ and $P90$ [17].

In conclusion, these measurements reveal CB changes which result from symmetry breaking in the ISF and $P30$ defects. They provide support for an extended, double period reconstruction model of the $P90$ core having many kinks. They rule out the ISF as a source of shallow, optically active states near the CB edge. Finally, they provide some insight into $P90$ dislocation motion and the role of kink formation by atomic pair rotation in the mobility of these dislocations.

Model structures for this work were relaxed by Y. Tu at IBM. I also acknowledge discussions with P. M. Mooney, F. K. LeGoues, and K. Ismail during this work. R. W. Nunes kindly provided atomic coordinates for the DP structure.

[1] L. C. Kimerling, H. J. Leamy, and J. R. Patel, Appl. Phys. Lett. **30**, 217 (1977).
[2] J. R. Patel and L. C. Kimerling, J. Phys. (Paris), Colloq. **40**, 67 (1979).
[3] H. Alexander, J. Phys. (Paris), Colloq. **40**, 1 (1979).
[4] A. Olsen and J. C. H. Spence, Philos. Mag. A **43**, 945 (1981).
[5] H. Alexander, J. C. H. Spence, D. Shindo, H. Gottschalk, and N. Long, Philos. Mag. A **53**, 627 (1986).
[6] V. Higgs, E. C. Lightowlers, C. E. Norman, and P. Knightley, Mater. Sci. Forum **83–87**, 1309 (1992).
[7] J. Weber, Solid State Phenom. **37–38**, 13 (1994).
[8] K. Ismail, F. K. LeGoues, K. L. Saenger, M. Arafa, J. O. Chu, P. M. Mooney, and B. S. Meyerson, Phys. Rev. Lett. **73**, 3447 (1994).
[9] Kai Shum, P. M. Mooney, and J. O. Chu, Appl. Phys. Lett. **71**, 1074 (1997).
[10] C. Weigel, H. Alexander, and J. W. Corbett, Phys. Status Solidi (b) **71**, 701 (1975).
[11] L. F. Mattheiss and J. R. Patel, Phys. Rev. B **23**, 5384 (1981).
[12] M. Y. Chou, M. L. Cohen, and S. G. Louie, Phys. Rev. B **32**, 7979 (1985).
[13] J. E. Northrup, M. L. Cohen, J. R. Chelikowsky, J. Spence, and A. Olsen, Phys. Rev. B **24**, 4623 (1981).
[14] J. R. Chelikowsky, Phys. Rev. Lett. **49**, 1569 (1982).
[15] J. R. Chelikowsky and J. C. H. Spence, Phys. Rev. B **30**, 694 (1984).
[16] J. Bennetto, R. W. Nunes, and David Vanderbilt, Phys. Rev. Lett. **79**, 245 (1997).
[17] R. W. Nunes, J. Bennetto, and David Vanderbilt, Phys. Rev. B **57**, 10 388 (1998).
[18] F. Liu, M. Mostoller, V. Milman, M. F. Chisholm, and T. Kaplan, Phys. Rev. B **51**, 17 192 (1995).
[19] S. J. Pennycook and L. A. Boatner, Nature (London) **336**, 565 (1988).
[20] R. F. Loane, E. J. Kirkland, and J. Silcox, Acta Crystallogr. Sect. A **44**, 912 (1988).
[21] P. E. Batson, Rev. Sci. Instrum. **57**, 43 (1986).
[22] P. E. Batson, Rev. Sci. Instrum. **59**, 1132 (1988).
[23] P. E. Batson, D. W. Johnson, and J. C. H. Spence, Ultramicroscopy **41**, 137 (1992).
[24] Y. M. Huang, J. C. H. Spence, and O. F. Sankey, Phys. Rev. Lett. **74**, 3392 (1995).
[25] P. E. Batson and J. F. Morar, Appl. Phys. Lett. **59**, 3285 (1991).
[26] J. F. Morar, P. E. Batson, and J. Tersoff, Phys. Rev. B **47**, 4107 (1993).
[27] P. E. Batson and J. F. Morar, Phys. Rev. Lett. **71**, 609 (1993).
[28] P. E. Batson, Ultramicroscopy **59**, 63 (1995).
[29] P. E. Batson, J. Electron. Microsc. **45**, 51 (1996).
[30] O. Zakharov, A. Rubio, X. Blase, M. L. Cohen, and S. G. Louie, Phys. Rev. B **50**, 10 780 (1994).
[31] M. V. Fischetti and S. E. Laux, J. Appl. Phys. **80**, 2234 (1996).